CrossMark

Exponential increase in the on–off ratio of conductance in organic memory devices by controlling the surface morphology of the devices

Giriraj Vyas[1] · Parveen Dagar[1] · Satyajit Sahu[1]

Abstract

We have shown an exponential increase in the ratio of conductance in the on and off states of switching devices by controlling the surface morphology of the thin films for the device by depositing at different rotational speeds. The pinholes which are preferred topography on the surface at higher rotational speed give rise to higher on–off ratio of current from the devices fabricated at the speed. The lower rotational speed contributes to higher thickness of the film and hence no switching. For thicker films, the domain is formed due to phase segregation between the two components in the film, which also indicates that the film is far from thermal equilibrium. At higher speed, there is very little scope of segregation when the film is drying up. Hence, there are only few pinholes on the surface of the film which are shallow. So, the filamentary mechanism of switching in memory devices can be firmly established by varying the speed of thin film deposition which leads to phase segregation of the materials. Thus, the formation of filament can be regulated by controlling the thickness and the surface morphology.

1 Introduction

Silicon-based switching devices are ubiquitous to any modern-day computer that exists around us. These switching devices are nothing but transistors. The processing capability of the computers depends on how many such switching devices are embedded in the integrated circuit (IC). Though the current processors have billions of transistors in them, still we thrive to achieve more in terms of performance by increasing the number exponentially. However, the number of transistors per square centimeter is close to the bottleneck and any further increase in the performance must be achieved by following an alternative technique. Organic switching devices may possibly be an alternative to resolve the bottleneck issue. Research on organic electronic devices such as light emitting diode [1, 2], solar cell [3, 4], photodetector [5], transistor [6, 7], spintronic materials [8] and photo controlled devices [9] has gained worldwide attention because of their flexibility to fabricate on any surface, cost effectiveness and easy solution processability [10]. Organic switching device, which is also called as organic memory device is also one such device which can be a replacement

for the silicon based switching device. Unlike silicon based transistor, this is based on the principle of resistive switching, wherein the device shows different conductance at a voltage bias.

The switching in the organic semiconductor based device is due to various reasons. One of the reasons for switching is the electrochemical oxidation and reduction of the material [11]. Here, the molecules are believed to be solely responsible for the switching in the device [12, 13]. A ferroelectric medium can also be used for the same purpose [14]. In case of resistive-switching device, there exists a resistive material in between two electrodes to form a metal insulator metal (MIM) structure [15]. By applying a voltage to the device, the resistance of the device changes by orders of magnitude. Devices made up of small molecules are also classified into the MIM structure [16–18]. Charge transfer complex formation also leads to switching in memory device [19]. Metallic nanoparticles in organic matrix were also studied and were found that the floating metallic island in the organic material is responsible for switching in the devices [20, 21].

Here, in this work, we have shown an exponential increase in the on–off ratio of conductance from switching devices consisting of a combination of an insulating polymer and a small molecule. This is primarily driven by the formation of metal filament. The filament formation can be validated by studying the surface morphology of the film used for device fabrication. The surface is filled with larger holes or smaller

✉ Satyajit Sahu
   satyajit@iitj.ac.in

1   Department of Physics, Indian Institute of Technology
    Jodhpur, Jodhpur, Rajasthan 342037, India

pinholes. The filaments through the pinholes give rise to consistent switching with high on/off ratio, but the on/off ratio is low in those devices where the holes are formed all over the surface. The formation of such structures on the surface of the film is dependent on the speed at which the spin-coated films are deposited.

2 Experimental section

For the fabrication of the devices, indium tin oxide (ITO)-coated glass substrates were used. They were procured from Techinstro, India. The ITO substrates were etched and cleaned using a standard cleaning procedure [22] which involves the following steps. The substrates are first etched using zinc dust and concentrated hydrochloric acid (HCl) by keeping a small stripe at the center of the substrate. These substrates are then ultrasonicated in soap solution followed by de-ionized water (DI) thrice for 15 min each in each solvent. Then a cycle of cleaning in ultrasonicator using Acetone and DI water for three times in each solvent and Methanol and DI water for three times in each solvent for the same amount of time as in soap solution. The substrates are then vacuum dried in an oven at 70 °C. The films were deposited on cleaned ITO substrates using spin-coating method. The active materials used for the deposition of film are 2,3-dichloro-5,6-dicyano-1,4-benzoquinone (DDQ) and poly(4-vinyl phenol) (PVP). The molecular structures of these materials are shown in Fig. 1a. All the chemicals are purchased from Aldrich Co. and used without further purification. The concentration of the solution was maintained at 25 mg/ml in isopropyl alcohol (IPA). We have chosen a weight ratio of 60:40 for DDQ and PVP in the solution for the fabrication of devices. The thin films were deposited at various spinning speeds starting from 1000 to 5000 rpm

with an increment of 1000 rpm. After deposition, the films are dried in vacuum in room temperature for 6–7 h. The devices will be ready to use after deposition of the top contact. Here the top metal contact is aluminum (Al) which is thermally deposited using a shadow mask. The thickness of deposited aluminum is 50 nm with an effective device area of 0.25 mm^2. So the devices have the following structure, i.e. ITO/DDQ:PVP/Al. A schematic of the device structure is shown in Fig. 1b.

The thickness of the deposited organic films was measured using Bruker Dektak XT-100 profilometer. It varied with respect to the spinning speed. For the 1000 rpm devices, the average thickness was 418 nm with a standard deviation of 34 nm, and for 5000 rpm devices, the average thickness was 106 nm with a standard deviation of 11 nm. The absorption spectrum for thin film as well as solution was recorded by Shimadzu UV1800 UV–visible spectrophotometer. The thin films were deposited on quartz substrate at the same rotational speed as those of the devices for the study of absorption spectra.

The surface morphology of the devices was studied using Park Systems XE-70 atomic force microscope (AFM). AFM was performed in a non-contact soft-tapping mode, and the scan rate was 0.4 lines per second. Total 256–512 such lines were there in a frame and the same number of pixels in each line. The cross-sectional scanning electron microscopic (SEM) images of all the devices fabricated at different rotational speeds were taken using a Zeiss EVO18 Scanning Electron Microscope (SEM). Electrical characterization of the devices was carried out in a homemade vacuum chamber having a base pressure of 1×10^{-5} mbar inside the chamber and with the help of a two-probe method using ITO and Al as bottom and top contacts, respectively. This allows us to nullify any effect of the oxides on the switching mechanism. The cross-bar architecture of the devices prevents the short circuit when a probe is brought in contact with the top Al electrode. The electrical study was performed using Keithley 6430 sub-femto-ampere source meter. Various characterizations were carried out on the samples including voltage sweep, long run endurance test, and repeated write–read–erase–read operations on the devices.
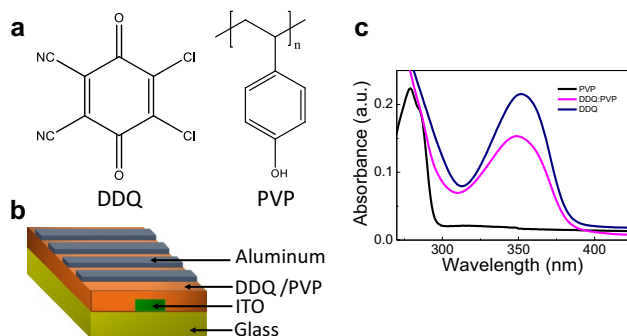
3 Results and discussion

3.1 Absorption spectra

The absorption spectra of the individual material in IPA were recorded, and for DDQ, the peak was observed at 352 nm, and for PVP, it appeared at 279 nm. The absorbance of the solution having both the materials suggests the presence of both the components. The peak intensity is dominated by DDQ, as can be seen in Fig. 1c. There is a

Fig. 1 **a** Molecular structure of DDQ and PVP molecules. **b** Schematic of device structure, where the top and bottom contacts are aluminum and ITO, the active layer is a combination of DDQ and PVP by a weight ratio of 60:40. **c** The absorption spectra of individual components along with the combination of DDQ and PVP in iso propyl alcohol

small hump due to the presence of PVP in the spectra. The solid-state absorption spectra of the thin films of the same samples give rise to slightly different peak positions. This is due to the difference in the order of crystallinity in the solid phase than the solution. This also establishes the fact that there is no charge transfer complex formation between the two organic materials, neither in solution nor in thin films.

3.2 Surface morphology study

From the AFM images shown in Fig. 2, it can be clearly seen that as the rotational speed of film deposition increased, the size of holes varies drastically from large holes to pinholes. For the 1000 rpm device, the average thickness was 418 nm with a standard deviation of 34 nm. At this speed, as shown in Fig. 2a, it is found that there exist only holes on the surface of the film. Here the sample started forming islands which are separated from each other and that leads to formation of holes. In some places, they even formed isolated structures. The gap between the islands is more than 1 µm, which is sufficient to form direct contact between the top and bottom electrodes. The study of 2000 rpm devices helps understand the surface morphology of the devices at this speed. The thickness for the device is approximately 245 nm. Figure 2b shows that the islands and structure formation

continue on the surface at this speed as well. Pinholes are still not present on the surface. Here the island boundaries are not separated from each other by a larger distance. The size of these varies from 400 to 500 nm which is sufficient to make direct contact between the top and bottom electrodes immediately after top metal contact is deposited. Therefore, at 1000 and 2000 rpm, the tendency to form isolated structure is more. In 3000-rpm-based device shown in Fig. 2c, structure formation is distinct as small (green circle), and big structures (red rectangle) are arranged in such a way that they do not give too much spacing in between them, hence the formation of filamentary pathways takes some time till it reaches a particular voltage bias. The thickness of the film is 161 nm. The film thickness decreases further at 4000 rpm as it is found to be approximately 151 nm. For films deposited at 4000 rpm, the surface is compactly filled with small structures of more or less same size as shown in Fig. 2d. The gap between the small structures is less than that obtained in 3000-rpm-based device. For 5000 rpm devices, the average thickness was 106 nm with a standard deviation of 11 nm. At the highest rotational speed of 5000 rpm of our study, it is found that the surface has only few pinholes as can be seen in Fig. 2e. These pinholes allow formation of metal filament very slowly till a particular voltage bias is applied.
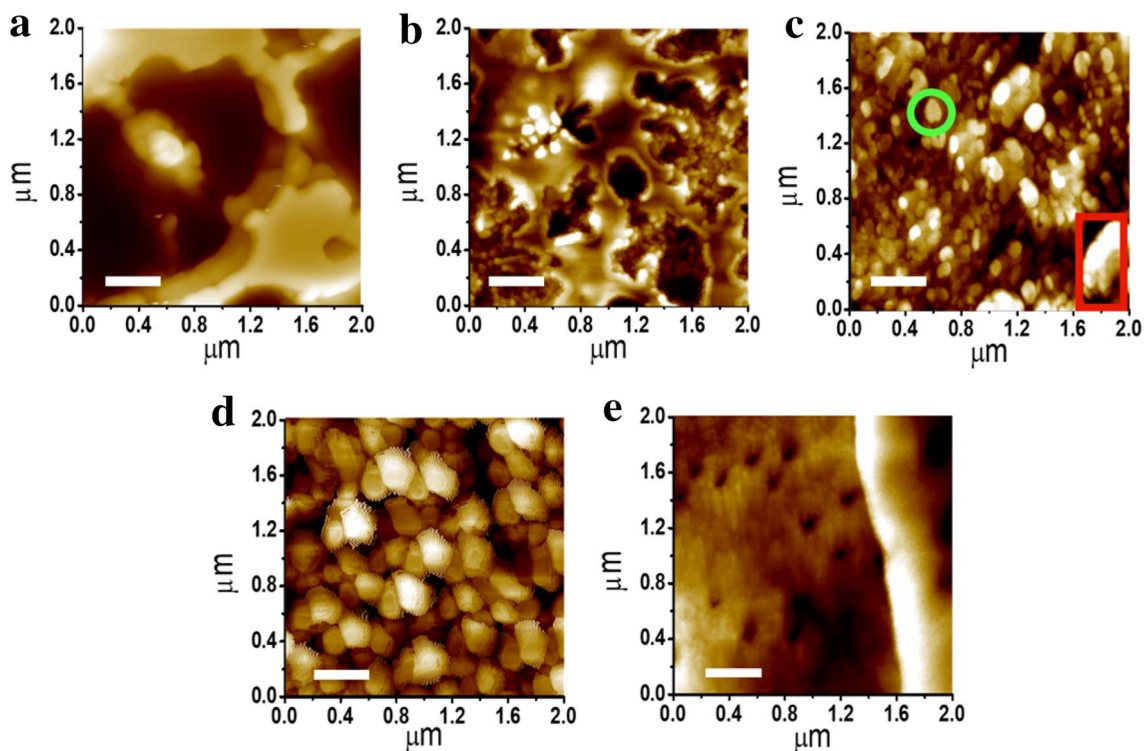

Fig. 2 The atomic force microscopy (AFM) topographic images of a spin cast films of combined material of DDQ and PVP deposited at 1000, 2000, 3000, 4000, and 5000 rpm, respectively. In **c**, the green circle and red rectangle show the small and larger particles on the non-uniform film surface. The scanned area for the images is $2 \times 2 \ \mu m^2$. Scale bar represents a length of 400 nm in all the images

For the devices, we also studied the cross-sectional SEM for devices fabricated at different rotational speeds. Figure 3a–e shows the cross-sectional scanning electron microscope (SEM) images of devices fabricated at 1000–5000 rpm, respectively, with an increment of 1000 rpm. The orange, yellow, and green color stripes represent aluminum (Al), active organic layer, and ITO, respectively, for each image. The yellow rectangle represents the area from where the energy dispersive X-ray (EDX) spectra were recorded. This area is part of the organic layer. The length scales are 200, 300, 200, 200 nm, and 1 μm, respectively, for images corresponding to (a)–(e). The energy dispersive X-ray spectra (EDX) obtained from the rectangular areas shown in the figures tell us the amount of aluminum penetrated the organic layer due to the formation of metal filaments through the holes/pinholes on the surface of the organic film. We also saw that film surface having holes on the surface such as the one prepared at 1000 rpm as in Fig. 3a, has a better contrast to imaging even at lower magnification. But, films prepared at higher speeds have smaller pinholes and hence relatively smoother surface, which is one of the reasons for not having very good contrast in the SEM images. The percentage of normalized atomic aluminum from 1000- to 5000-rpm-based devices in the organic layer was 5.62, 4.2, 0.97, 0.9, and 4.49%, respectively.

3.3 Study of *I–V* characteristic curve

The *I–V* characteristic curves for the devices showed interesting behavior. The 1000-rpm-based device shows no switching as can be seen in Fig. 4a, the *I–V* curve almost goes linearly with a very high current on both positive and negative bias directions. The dashed arrows guide the direction of voltage scan. At even higher rotational speed, i.e., at 2000 rpm, though the device shows semiconducting behavior, it does not feature switching in either positive or negative voltage bias as can be seen in Fig. 4b. Hence, the on–off ratio is very less. In case of 3000 rpm devices, it showed significant switching in the negative direction of applied voltage bias as seen in Fig. 4c. The highest on–off ratio for the device is 4.8×10^2. For 4000-rpm-based device, the switching continues to be on the negative side with an on–off ratio of 2.4×10^3 as seen in Fig. 4d. At 5000 rpm, the device continued to show switching in the negative direction with a maximum on–off ratio of 1.2×10^4 as can be seen in Fig. 4e. The dashed arrows in the figure show the direction of voltage scan for the device. In all the devices, the switching behavior is consistent with high reproducibility. Therefore, the on–off ratio for the devices varied exponentially with the increase in rotational speed of deposition of the films as shown in Fig. 3f. We have tested close to 50 devices for each speed and ran 100 s of *I–V* curves for each device. The reproducibility for the *I–V* curves is more than 90%.

3.4 Mechanism of switching in the devices

The exponential increase in the on–off ratio of the current can be used to give an excellent description of switching by metal filament formation. To start with the lowest rotational speed (1000 rpm) for the fabrication of device, we observed big holes on the surface which can be potential sites for the direct contact of the top and bottom electrodes. This can be
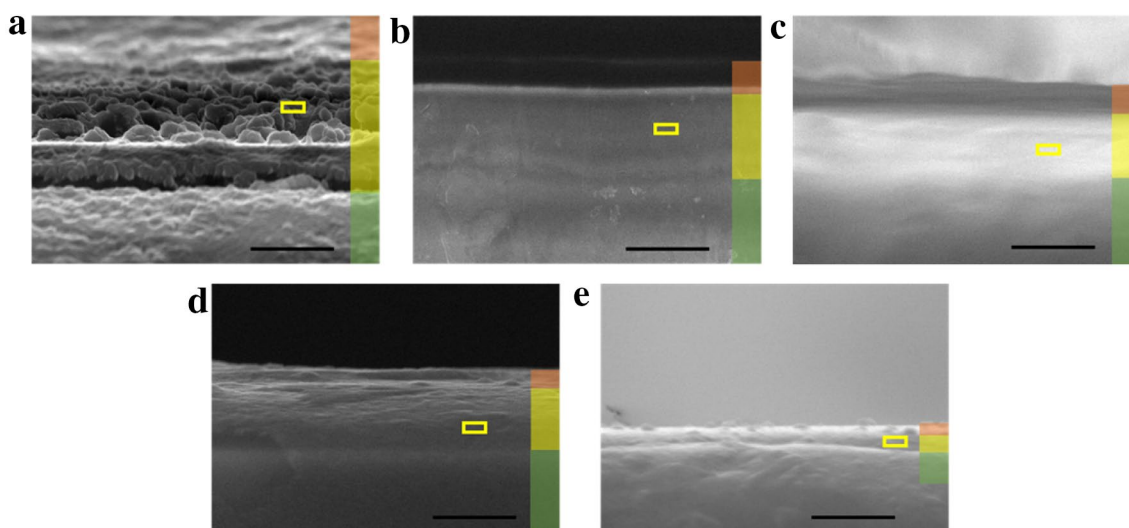

Fig. 3 Cross-sectional scanning electron microscope (SEM) images of devices fabricated at 1000 to 5000 rpm, respectively, with an increment of 1000 rpm. The orange, yellow, and green color stripes represent aluminum (Al), active organic layer, and ITO, respectively, for each image. The yellow rectangle represents the area from where the EDX was recorded. This area is part of the organic layer. The length scales for the images are 200, 300, 200, 200 nm, and 1 μm, respectively, for images corresponding to **a–e**
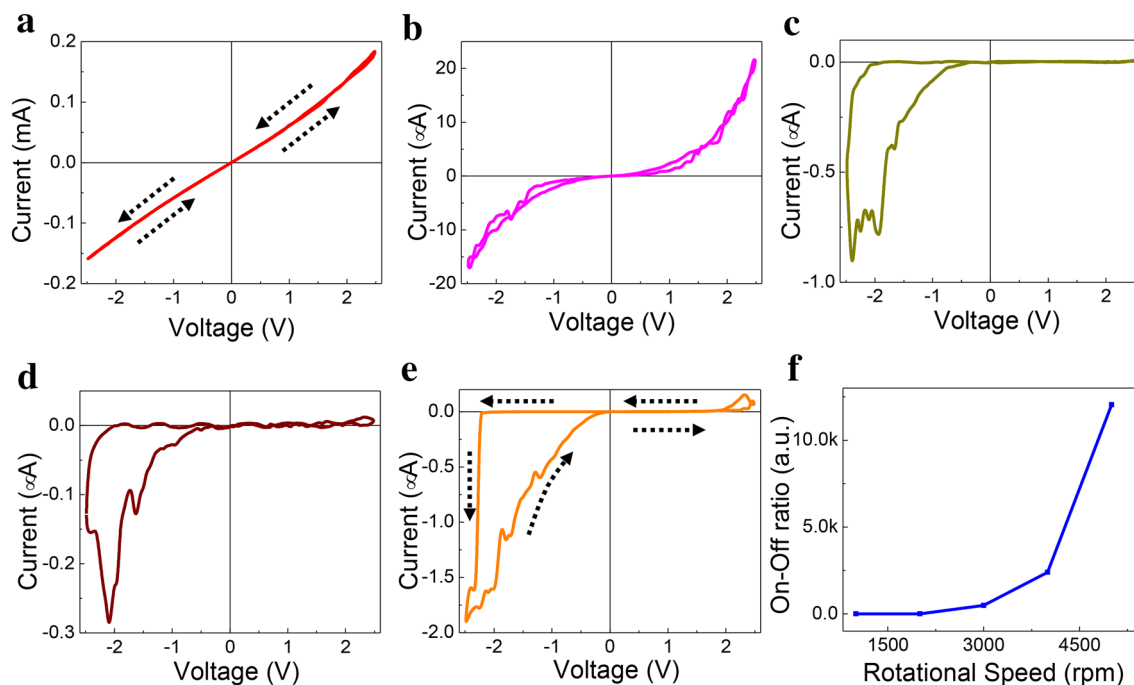
Fig. 4 *I–V* characteristic curves from the devices fabricated at 1000, 2000, 3000, 4000, and 5000 rpm, respectively. The dotted arrows in **a** and **e** show the direction of the voltage scan. **f** The variation of on–off ratio of current with respect to rotational speed

proven from the *I–V* characteristic curves, which repeatedly showed linear behavior with very high order of current. This ohmic behavior is only possible for conductors, which in this case are the channel formed between the top and bottom contacts, and mostly formed by the top aluminum contact. The authors have already shown the formation of metal filament formation using thermal imaging of the device while scanning the *I–V* curves [22]. This is shown in Fig. 5a which depicts the proposed mechanism for conduction in this device. Figure 5b describes the mechanism behind the operation of device fabricated at 2000 rpm. In this device, since the holes on the surface are smaller than the device prepared at 1000 rpm, the probability of formation of direct metal contact is less and this is perceived from the *I–V* curve as it is nonlinear, and the order of current is also much lower than before. Since there is no switching from the device which has same materials as other devices, there is a possibility of formation of direct metal contact between the two electrodes, albeit much narrower than before which proportionally decreases the conductance, and hence the current in the *I–V* characteristic curve.

For devices fabricated at 3000 rpm, the surface looks free from holes but certainly filled with cracks covered with small structures, which are not uniform in size. These cracks are prone to metal filament formation, but at some higher driving voltage. This is because, the cracks may be being so narrow that direct contact between the top and bottom contacts may not happen immediately after deposition of

top aluminum contact though the film is thinner than the previous devices. At a particular bias in the negative direction, the migration of metal ions from the top to the bottom contacts started because of the high electric field between the two contacts, and continues till a direct contact is made at some higher voltage, at which point the conductance goes high. This "sets" the device and it will continue to be in the high conducting state while traversing back from high to low voltage direction till the conductance comes down when the filament breaks and hence "resets" the device. The on–off ratio for the device is not high as the off-state (low conducting state) current is high because of the partial conducting channel between the two contacts. Figure 5c depicts schematically the operational mechanism behind the device.

At still higher rotational speed (4000 rpm), the film deposited has a surface covered with uniformly distributed small structures. Since the cracks are not as distinct as in 3000 rpm films, the penetration of aluminum in the film will be less than before and hence the off-state current is low, but since the thickness of the film is more or less same as before, the voltage at which the transition from low to high conducting states occurs is almost same as in 3000-rpm-based device. Figure 5d indicates the metal ions in the form of small spheres. At the highest rotational speed (5000 rpm) for film deposition in our study, it can be seen that the film surface has pinholes scattered sparsely. These pinholes are sites for metal filament formation. They will not allow the migration of aluminum easily through them; hence there is no smooth transition from the low to high

Fig. 5 The model representation to describe the operation mechanism of devices fabricated at 1000, 2000, 3000, 4000, and 5000 rpm, respectively. In **a**, the gray color channel is having a much wider opening at the aluminum contact side. In **b**, the opening of the channel is much smaller than 1000-rpm-based device with a wider central region. In **c**, the opening as well as the middle regions get much narrower. In **d** and **e**, the gray balls represent small metal ions from the contact. The color coding is same as in Fig. 1b
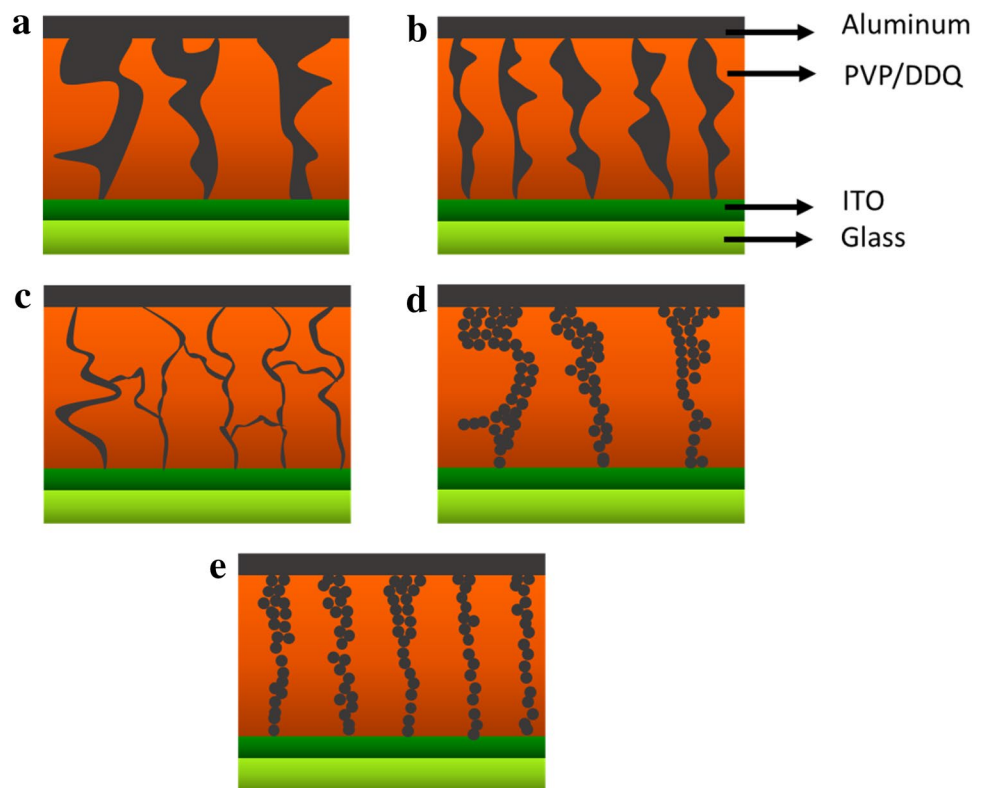
conducting states. The transition occurs at a particular voltage, which is the threshold voltage for switching. At this voltage, the percolating path between the top and bottom contacts is continuous for the metal ions. The *I–V* curve is reproducible in multiple scanning loops. The device remains in the high conducting state even in the returning path of the *I–V* scan. Here the off-state current is low but there is an order of increase in the on-state current as the resistance of the device might have decreased because of the decrease in path length of the filament. Therefore, this significantly increased the on–off ratio of current between the high and low conducting states as can be seen in Fig. 4f. The observation that formation of filament leads to the switching in the devices can also be proven from the EDX data, where the percentage of normalized atomic aluminum in the organic layer of the devices is decreasing with the increase in rotational speed. This is because with the decrease in the size of the holes the passage for aluminum into the holes becomes difficult, therefore less amount of aluminum will enter into the holes and hence a trend in decrease of atomic aluminum in the organic layer of the device.

3.5 Influence of surface morphology on *I–V* characteristics

Therefore, the exponential increase in the on–off ratio across devices having films of a combination of DDQ and PVP prepared with varied rotational speed is due to the morphology of the films. The topography of the films changed, with bigger holes in thicker films and pinholes in thinner films. The thickness of the film is inversely proportional to the rotational speed at which the films are deposited [23]. Since the substrate and solvent for all the films prepared for devices are same, the difference in surface morphology must be due to some parameters associated with thickness of the films. For thicker films, the domain is formed due to phase segregation between the two components in the film, which also indicates that the film is far from thermal equilibrium though all the films are dried at same temperature after deposition. This is because thicker films take longer time to dry which leads to longer diffusion time and higher degree of domain formation time during spin coating [23, 24]. At higher speed, there is very little scope of segregation when the film is drying up. Hence, there are only few pinholes on the surface of the film which are shallow.

3.6 RAM and ROM application of the switching devices

The device fabricated using thin film deposited at 5000 rpm is tested for various memory applications, such as random-access memory (RAM) and read only memory (ROM). To study the RAM feature of the device, a cycle of write–read–erase–read voltage pulse at -4, -1.5, 4, -1.5 V for 5, 10, 5, and 10 s, respectively, was run for more
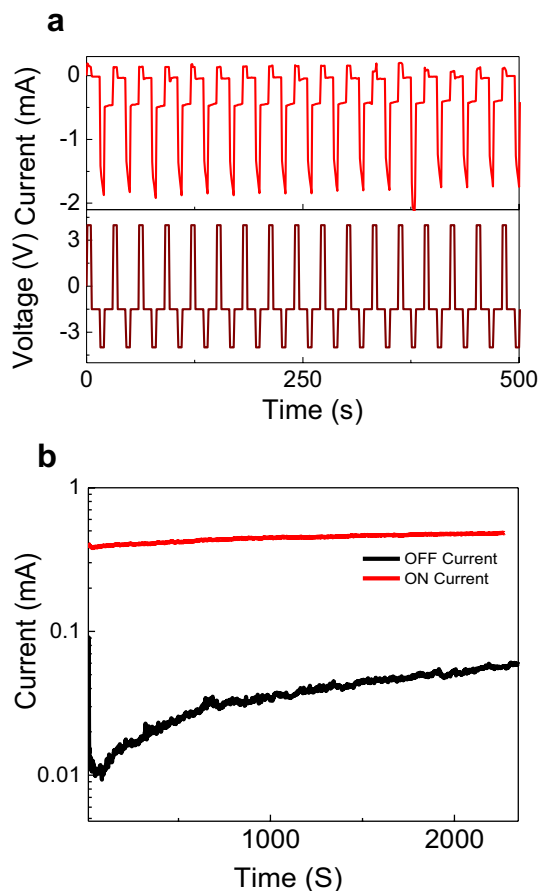
Fig. 6 The write–read–erase–read voltage pulse cycle shows the variation of current with respect to time after a write voltage $V_{write} = -4$ V, erase voltage, $V_{erase} = 4$ V and read voltage $V_{read} = -1.5$ V are applied for 5, 5, and 10 s, respectively. **b** The variation of current with respect to time at a fixed read voltage pulse of -1.5 V, after being written and erased at -4 and 4 V for 5 s, respectively. The train of current at -1.5 V followed by write and erase voltage pulses are called as on and off state current and are measured for more than 2000 s

than 1000s, and it was found to read the state reproducibly without any decay as shown in Fig. 6a. The rate of writing and reading is -4 and 4 V/s, whereas the reading speed is -1.5 V/s. Similarly, the ROM feature was studied by probing the high and low conducting states after writing and erasing the states. The write voltage pulse of -4 V was applied for 5 s and then the state was read by a voltage pulse of -1.5 V for more than 2×10^3s, similarly, erase voltage pulse of 4 V was applied for 5 s and then the state was read by a voltage pulse of -1.5 V for more than 2×10^3 s. Here we have considered the absolute values of current. In both cases, the device showed good stability as can be seen from Fig. 6b. We have chosen a higher write and erase voltage pulses because the read states are more stable after these voltage pulses.

4 Conclusion

Therefore, we have studied switching devices fabricated at different rotational speeds using spin-coating method. The devices are having different thicknesses and surface morphology. The thickness of the devices decreased with increase in rotational speed. The surface topography of the thin films used for device fabrication varied from being rough and non-uniform to smooth and uniform. The rough surface prepared at lower rotational speed had holes and domains in it, whereas the films prepared at highest rotational speed had pinholes in them. Therefore, the phase segregation which is proportional to the speed of rotation is the reason that leads to the change in surface morphology. The variation of surface topography leads to an exponential increase in the on–off ratio from the switching devices, and hence provides an option to achieve higher on–off ratio from devices by controlling the rotational speed during device fabrication.

References

1. C.W. Tang, S.A. VanSlyke, Appl. Phys. Lett. **51**, 913 (1987)
2. M. Strukelj, R.H. Jordan, A. Dodabalapur, J. Am. Chem. Soc. **118**, 1213 (1996)
3. S.E. Shaheen, C.J. Brabec, N.S. Sariciftci, F. Padinger, T. Fromherz, J.C. Hummelen, Appl. Phys. Lett. **78**, 841 (2001)
4. B.A. Gregg, J. Phys. Chem. B **107**, 4688 (2003)
5. P. Peumans, V. Bulović, S.R. Forrest, Appl. Phys. Lett. **76**, 3855 (2000)
6. C.D. Dimitrakopoulos, P.R.L. Malenfant, Adv. Mater. **14**, 99 (2002)
7. S.-J. Kim, J.-S. Lee, Nano Lett. **10**, 2884 (2010)
8. K.S. Kumar, M. Ruben, Coord. Chem. Rev. **346**, 176 (2017)
9. M. Suda, Bull. Chem. Soc. Jpn. **91**, 19 (2017)
10. J. Zhang, W. Xu, P. Sheng, G. Zhao, D. Zhu, Acc. Chem. Res. **50**, 1654 (2017)
11. Q. Li, G. Mathur, S. Gowda, S. Surthi, Q. Zhao, L. Yu, J.S. Lindsey, D.F. Bocian, V. Misra, Adv. Mater. **16**, 133 (2004)
12. Z. Liu, A.A. Yasseri, J.S. Lindsey, D.F. Bocian, Science (80-.) **302**, 1543 (2003)
13. K.M. Roth, J.S. Lindsey, D.F. Bocian, W.G. Kuhr, Langmuir **18**, 4030 (2002)
14. T. Furukawa, Phase Transit. A Multinatl. J. **18**, 143 (1989)
15. M. Kiguchi, S. Fujii, Bull. Chem. Soc. Jpn. **90**, 1 (2016)
16. J. Kevorkian, M.M. Labes, D.C. Larson, D.C. Wu, Discuss. Faraday Soc. **51**, 139 (1971)
17. A. Bandyopadhyay, A.J. Pal, Appl. Phys. Lett. **82**, 1215 (2003)
18. A. Bandyopadhyay, A.J. Pal, Appl. Phys. Lett. **84**, 999 (2004)

19. Z. Liu, F. Xue, Y. Su, K. Varahramyan, IEEE Electron Device Lett. **27**, 151 (2006)
20. L. Ma, J. Liu, S. Pyo, Y. Yang, Appl. Phys. Lett. **80**, 362 (2002)
21. L.P. Ma, J. Liu, Y. Yang, Appl. Phys. Lett. **80**, 2997 (2002)
22. G. Vyas, P. Dagar, S. Sahu, Appl. Phys. Lett. **108**, 233301 (2016)
23. F. Zhang, C. Di, N. Berdunov, Y. Hu, Y. Hu, X. Gao, Q. Meng, H. Sirringhaus, D. Zhu, Adv. Mater. **25**, 1401 (2013)
24. S. Walheim, M. Böltau, J. Mlynek, G. Krausch, U. Steiner, Macromolecules **30**, 4995 (1997)